

Collagen Architecture of the Posterior Pole: High-Resolution Wide Field of View Visualization and Analysis Using Polarized Light Microscopy

Ning-Jiun Jan,^{1,2} Kira Lathrop,^{1,2} and Ian A. Sigal^{1,2}

¹Department of Ophthalmology, University of Pittsburgh, Pittsburgh, Pennsylvania, United States

²Department of Bioengineering, University of Pittsburgh, Pittsburgh, Pennsylvania, United States

Correspondence: Ian A. Sigal, Laboratory of Ocular Biomechanics, Department of Ophthalmology, University of Pittsburgh Medical Center, 203 Lothrop Street, Room 930, Pittsburgh, PA 15213, USA; ian@OcularBiomechanics.com.

Submitted: September 17, 2016
Accepted: December 18, 2016

Citation: Jan NJ, Lathrop K, Sigal IA. Collagen architecture of the posterior pole: high-resolution wide field of view visualization and analysis using polarized light microscopy. *Invest Ophthalmol Vis Sci.* 2017;58:735–744. DOI:10.1167/iovs.16-20772

PURPOSE. The purpose of this study was to leverage polarized light microscopy (PLM) to visualize the collagen fiber architecture of posterior pole and optic nerve head with micrometer-scale resolution and to identify and quantify major organizational components.

METHODS. Eight sheep posterior poles were cryosectioned and imaged using PLM. Collagen fiber orientation was determined by using custom scripts, and the resulting orientation maps were inspected and quantified to identify major structural elements and tested for differences in mean fiber orientation and anisotropy, using linear mixed effect models.

RESULTS. Images revealed an intricate organization of collagen fibers in the posterior pole. In the lamina cribrosa, interweaving fibers formed large knots and wrapped around nerve fiber pores, with beam insertions into the scleral canal wall that were either narrow and straight or wide. In the peripapillary sclera, three significantly different ($P < 0.0001$) components were identified: fibers oriented circumferentially proximal to the canal, radially in the innermost sclera, and unaligned with interweaving fibers. The radial fibers were between 60 and 180 μm thick, extending at least 3 mm from the canal.

CONCLUSIONS. PLM revealed structural aspects of the lamina cribrosa and sclera that may have important biomechanical roles but that were previously unreported or not characterized quantitatively. In the lamina cribrosa, these roles included wide and narrow beam insertions and details of collagen fibers interweaving and wrapping around the pores. In the sclera, we described regions of circumferential, radial, and unaligned “random” fibers. Although there is consensus that circumferential fibers protect neural tissues by resisting canal expansion, the role of the radial fibers remains unclear.

Keywords: collagen, lamina cribrosa, microscopy, optic nerve head, sclera

The collagen fibers of the connective tissues of the eye play a central role in determining the biomechanical behavior of the globe and are therefore central to eye physiology and pathophysiology.^{1,2} Hence, to understand the eye and preserve vision, it is necessary to characterize the architecture of collagen fibers. Multiple techniques have been deployed toward this goal, including small-angle light scattering (SALS),^{3,4} X-ray scattering,^{5–8} nonlinear,^{9,10} scanning electron,^{11–13} and transmission electron¹⁴ microscopies, and magnetic resonance imaging (MRI).^{15,16} These techniques, although useful, have one or more of the following limitations, such as a small field of view, low resolution, subjective and slow analysis, high expense, and introduction of artifacts. Collagen fiber architecture has also been predicted using inverse numerical modeling.^{17,18} These models are particularly useful because they can predict essential properties of the collagen fibers, such as fiber waviness or crimp, which the experimental techniques mentioned above have not provided.¹⁹ However, inverse model predictions remain to be validated, in part because of a lack of suitable experimental techniques.

We recently demonstrated a technique based on polarized light microscopy (PLM) that can provide accurate, robust, and repeatable measurements of ocular collagen fibers.²⁰ Our goal

in this work was to leverage PLM to visualize and quantify, with micrometer-scale resolution, the distribution and orientation of collagen in the posterior sclera and optic nerve head (ONH), and to identify the major organizational components of these regions at the macroscopic, whole-tissue scale.

METHODS

Specimen Preparation

Eight eyes from 5 adult (~2-year old) sheep were obtained from the local abattoir and processed within 8 hours after death. The globes were cleaned by carefully removing the fat, muscles, and episcleral tissues, using scalpels, razors, and forceps. The eyes were cannulated through the anterior chamber and fixed overnight with 10% formalin while maintaining a controlled IOP of 5 mm Hg or 50 mm Hg by both perfusion and immersion. A total of 7 eyes were fixed at an IOP of 5 mm Hg, whereas 1 eye was fixed at an IOP of 50 mm Hg. Posterior pole regions centered on the ONH were excised using a circular trephine (either 8-mm or 11.5-mm diameter) and cryosectioned coronally into 30- μm -thick sections. Note that no labels or stains were applied and the tissues were never dehydrated. The



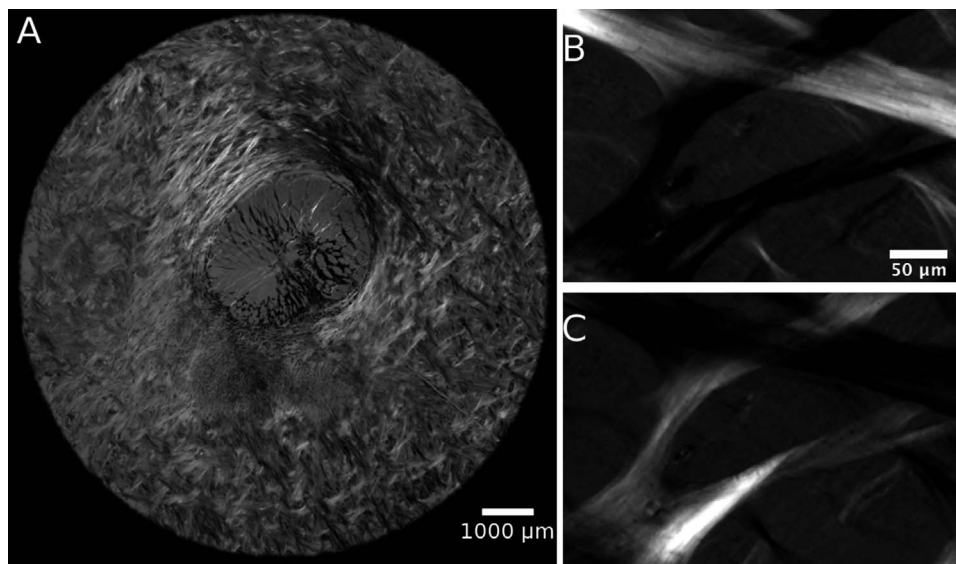


FIGURE 1. PLM images of the posterior pole. Raw PLM images of a section of optic nerve head show different intensities for collagen fibers oriented in different directions (A). Two PLM images of lamina cribrosa beams with the polarizer changed by 45° (B, C).

tissues were not flattened, and we did not make stress-relieving cuts that could affect collagen orientations.⁵ Elsewhere we have shown that the tissue processing described above with 10% formalin followed by sectioning has minimal effects on tissue shape or size (e.g., mean ONH area changed by less than 2.5% without a change in circularity) (Tran H, manuscript submitted, 2017).

Measuring Collagen Orientation

The local collagen orientation was determined from images captured using PLM following protocols previously reported.²⁰ Briefly, a white light source and two polarizing filters were used (Hoya, Tokyo, Japan). The birefringence of the collagen fibers causes the intensity of the detected light to vary depending on the relative orientation of the fiber and the direction of polarization of the light (Fig. 1). Thus, local collagen orientation at each pixel can be determined from multiple images captured with different relative orientations.²⁰

Image Acquisition

Three imaging methods were used. Two methods used for visualization of lamina cribrosa and sclera, respectively, are described below. The third method used for further analysis of the sclera is described later in Methods in the subsection on quantification. The rationale for the choices and merits of each method are presented in Discussion.

The lamina cribrosa was captured using a 10× objective (numerical aperture [NA], 0.3) on a model BX60 microscope (Olympus, Tokyo, Japan), using an RT Slider camera (SPOT Imaging Solutions, Sterling Heights, MI, USA). Sections from 2 eyes, 1 fixed at 5 mm Hg IOP (11.5 mm diameter trephine) and 1 fixed at 50 mm Hg IOP (8 mm diameter trephine), were imaged (12-bit grayscale, 0.73 µm/pixel). To capture the whole lamina cribrosa, 20 to 35 images with 20% overlap were captured for each section using a manual stage and stitched into mosaics using Fiji Is Just ImageJ (FIJI).²¹

The peripapillary sclera was imaged using a 10× objective (NA, 0.5) on an Eclipse Ti model microscope (Nikon, Melville, NY, USA), with a Cascade 1K camera (Roper Scientific, Sarasota, FL, USA). Sections from two eyes fixed at 5 mm Hg IOP (11.5 mm diameter trephine) were imaged (16-bit

grayscale, 0.80 µm/pixel). To capture the whole section in submicrometer-resolution, we used MetaMorph software (Molecular Devices, Sunnyvale, CA, USA) paired with a motorized x-y stage to capture a mosaic. For each section, stitched image sets of 80 to 125 images were automatically captured and stitched.

Image Presentation

The ability to understand collagen fiber organization and identify the main features of their architecture depends on the methods used for visualization. Below we describe several tools used toward this goal.

A masking technique was applied to help distinguish tissues in which the local fiber orientation at a pixel is weighted by an “energy” parameter, as described elsewhere.²⁰ Energy was defined by the equation $energy^2 = (I_{90} - I_0)^2 - (I_{135} - I_{45})^2$, where I_α was the pixel intensity at relative angle α between sample and polarizing filters. Energy is large when there is substantial information on collagen fiber orientation and small when there is little information. Little information would occur, for example, in regions without tissues or where pigment blocks the signal. Energy weighting substantially improved visualization of structure at large (Fig. 2), medium, and small scales (Fig. 3). Unless indicated otherwise, images of orientation are shown with energy weighting. Quantitative analyses were done without weighting.

Visualization of local fiber orientations was also enhanced by plotting short line segments to indicate the mean collagen fiber orientation within a small region (also referred to as a kernel). These were particularly helpful when also weighted using the energy parameter mentioned above, as this makes lines more intense and visible in areas with high signal quality and fade to dark in areas outside the tissues or occluded by pigment (Fig. 3).

Visualization of the larger scale organization of the collagen fibers was enhanced by using a “tracing method” similar to the nerve fiber tracings used in MRI-based diffusion tensor imaging (Fig. 4).¹⁵ The traces started by generating a set of seed points. From each seed point the algorithm produced a trace using local collagen orientation following a Euler integration scheme²² with step size an order of magnitude smaller than pixel size. Tracing stopped if local energy decreased under a

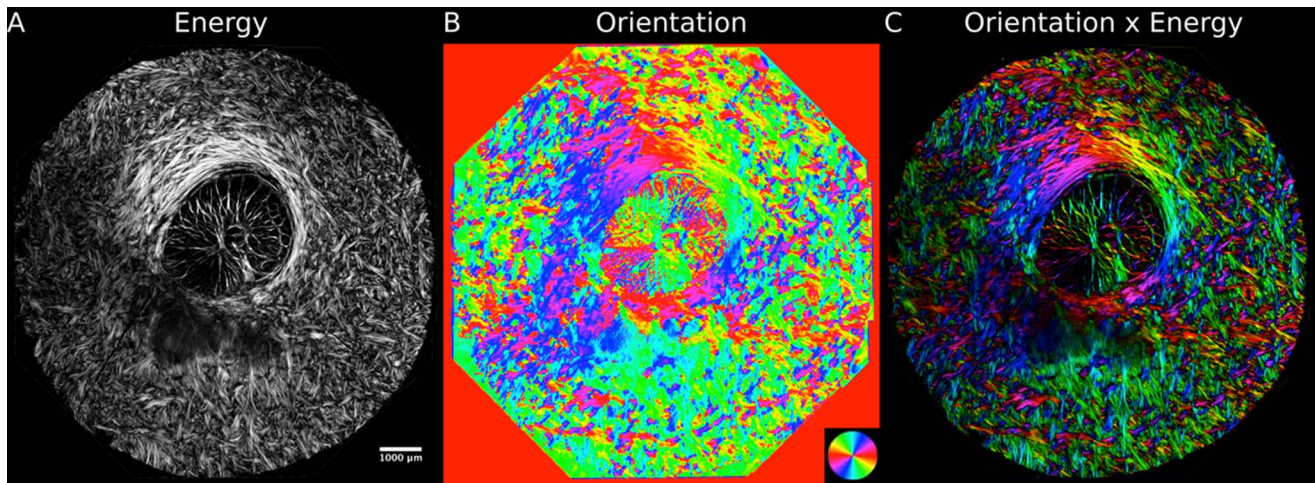


FIGURE 2. Improving collagen structure visualization by applying a mask. Scaling intensity by energy (A) helps distinguish the collagen fibers from regions outside the tissues. By using this energy scaling to “mask” color maps of the collagen fiber orientation (B), the architecture of the collagen fibers can be better understood (C).

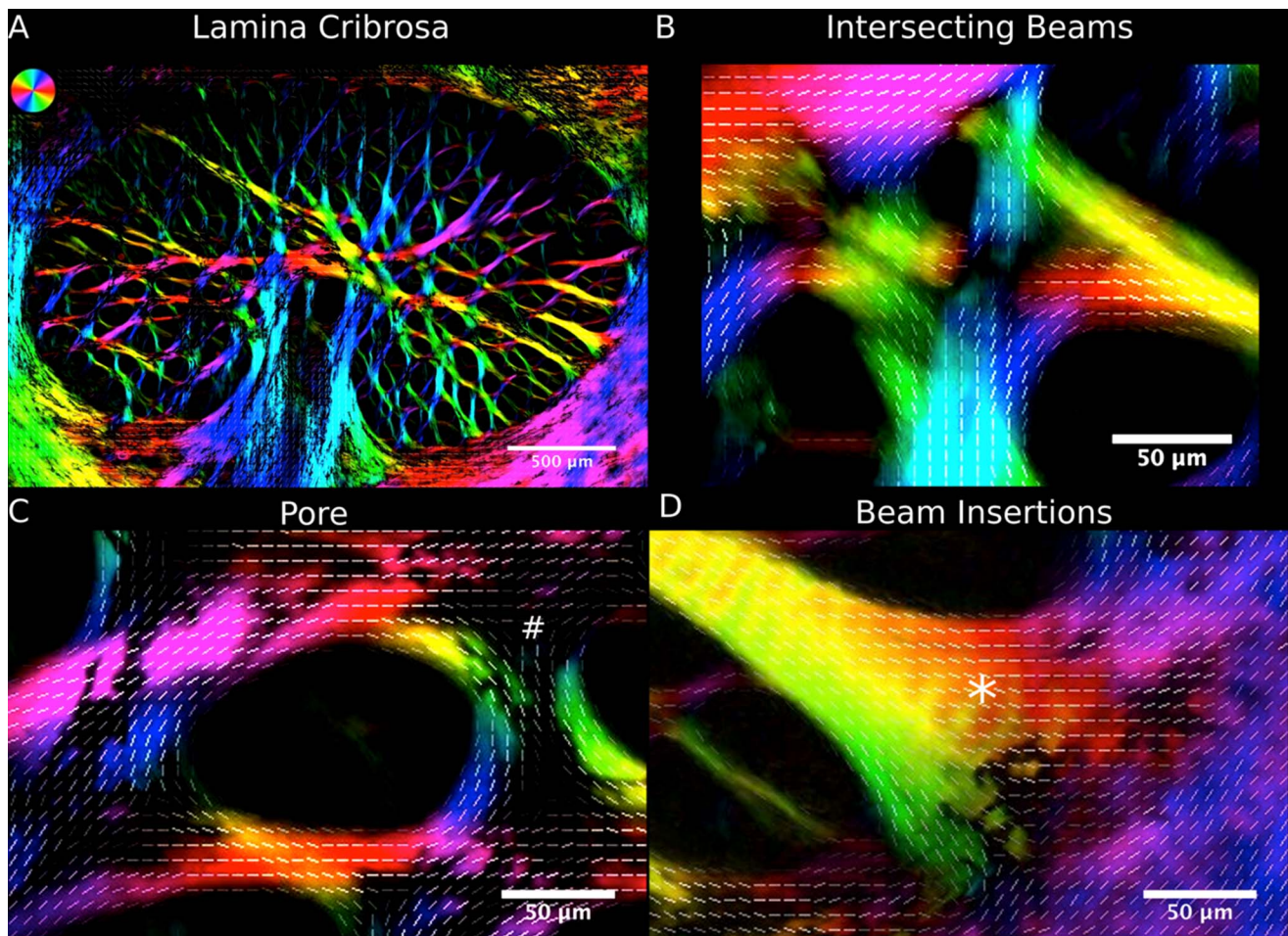


FIGURE 3. The lamina cribrosa visualized on a submicrometer scale, using PLM. The collagen microarchitecture of the lamina cribrosa (A) is complex, with “knots” of intersecting beams (B), fibers wrapping circumferentially around pores (C), and anchor points where the lamina cribrosa inserts into the scleral canal (D). Dark regions of low energy due to pigment can be seen within the sclera ([A] top right) and beams ([C] hashtag) and sclera but did not impede orientation calculations (white overlaid orientation lines, averaged over $3 \times 3 \mu\text{m}^2$). High spatial and angular resolution allows identification of crimp, or the natural waviness of the collagen fibers, as color oscillations, such as the yellow and red bands in the beam insertion ([D] asterisk). These images were acquired from sections of an eye fixed at 5 mm Hg.

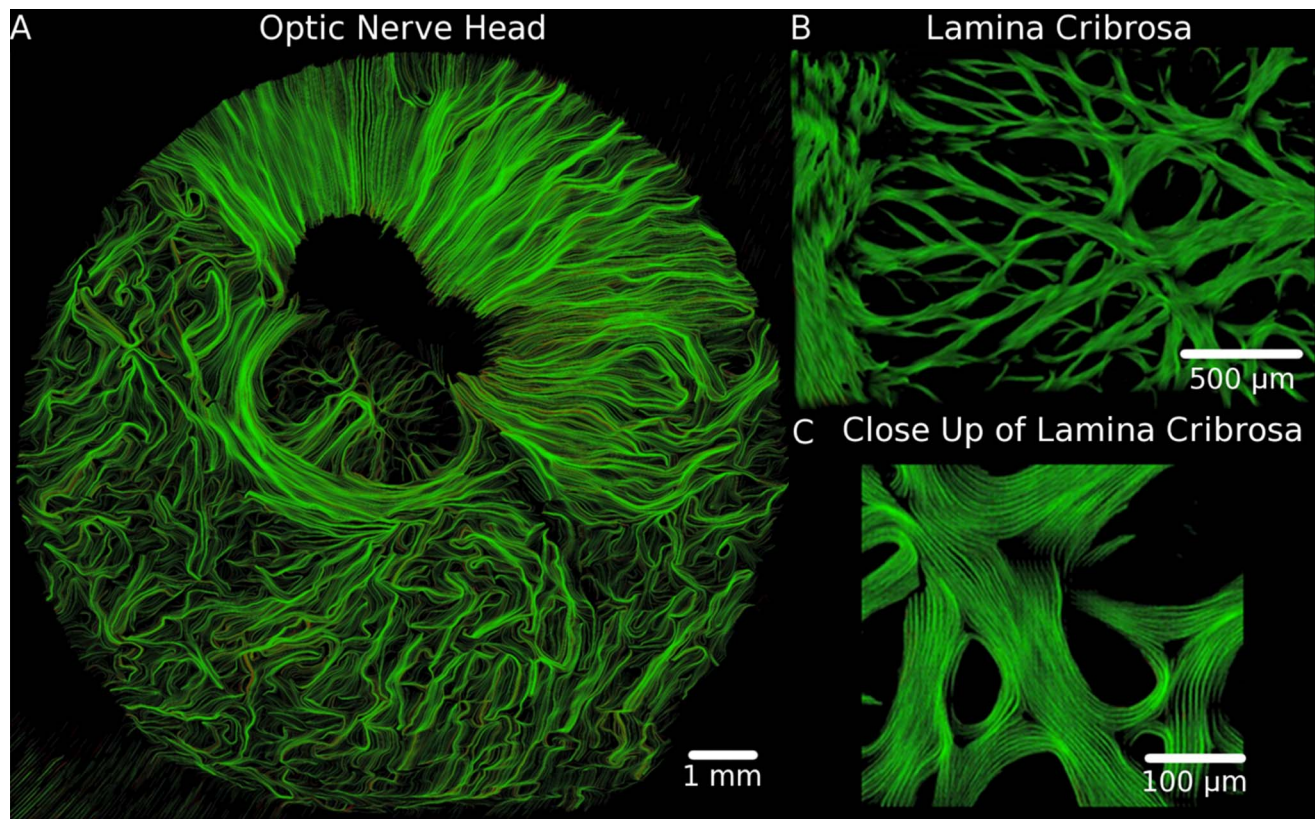


FIGURE 4. Traces of the collagen fibers in the optic nerve head at different magnifications help visualize the continuity of the fibers and their regional anisotropy. Longer, more aligned lines indicate a region of higher anisotropy. (A) Highly anisotropic regions in the sclera appeared as well organized fibers that either wrapped circumferentially around the canal or extended radially from the canal to the edge of the section. (B) In the lamina cribrosa, the traces revealed the complex network of collagen fibers and (C) show how the fibers intersect and wrap around the lamina cribrosa pores. These images were acquired from sections of an eye fixed at 50 mm Hg. Because this coronal section is slightly tilted, the *top right* part of the section is more anterior, whereas the *lower left* part of the section is more posterior. The *black region* next to the canal is an area anterior to the sclera, with high content of pigment and either low or no collagen.

set threshold (usually approximately 0.1) or if the trace were to take a sudden change in direction greater than 45° over a few pixels. In addition, after a specified maximum length, the trace ends in order to avoid overcrowding. Note that this tracing algorithm was only intended as a visualization aid and that there should be no expectation that it is following a single fiber, fiber bundle, or lamella.

Quantifying Peripapillary Scleral Collagen Architecture

While inspecting the maps of peripapillary sclera collagen fiber orientation, we noticed that there appeared to be 3 distinct regions according to the fiber architecture: i) the collagen in the scleral canal immediately adjacent to the lamina cribrosa oriented circumferentially around the canal forming a ring of fibers²³; ii) a thin layer in the innermost sclera with collagen fibers oriented radially from the scleral canal perpendicular to the ring; and iii) the rest of the sclera formed by interweaving collagen bundles that did not have a clear main orientation (Fig. 5). Hence, we set out to determine whether these apparently different regions were indeed significantly different and whether they are present in all eyes.

Analysis of sclera was conducted using images captured on the $1\times$ objective (NA 0.1) of a model SMZ1500 microscope (Nikon) paired with a DXM1200 camera (Nikon). This microscope-camera pair allowed imaging of the whole section without mosaicking. An average of 75 serial sections (range, 42

to 154 sections) from 7 eyes from four sheep fixed at 5 mm Hg IOP were imaged (32-bit RGB, $4.1\ \mu\text{m}/\text{pixel}$). From these images, rectangular areas (300- to 600- μm side length) representative of each of the three regions were manually marked in every section image, when discernible. For analysis, the orientations were converted into polar coordinates based on a manually identified center of the scleral canal. In this system, 0° represented a radial orientation and 90° a circumferential orientation. For this study, we took deviations from radial in either direction to be equivalent. For each area marked (674 total), we computed the mean fiber orientation and the circular variance using directional statistics as a measurement of degree of alignment or anisotropy.²⁴ To simplify interpretation, the anisotropy was normalized by the value of a uniform distribution and the value subtracted from 1. Thus, an anisotropy of 1 represents perfectly aligned fibers, whereas an anisotropy of 0 represents fibers perfectly splayed in all directions, such as in a random distribution. Directional statistics of this type are well established and common in the study of orientation parameters.²⁵

Statistical Analysis

A linear mixed effects model was fit to test whether mean angle and fiber anisotropy were significantly predicted by region, accounting for autocorrelations between measurements taken from the same sections, eyes, and individuals.

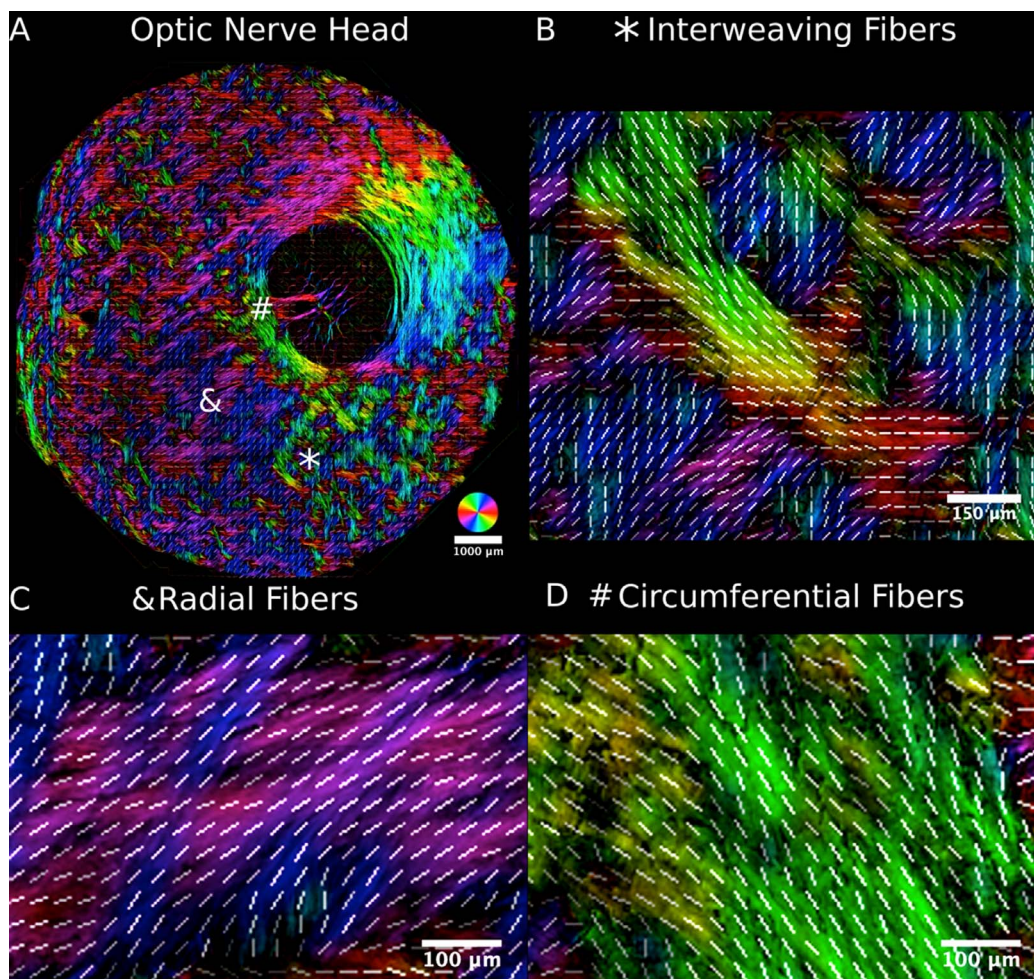


FIGURE 5. The peripapillary sclera visualized on the submicrometer scale using PLM. Three major organizational patterns were identified and marked by an *asterisk* (A), an *ampersand*, and a *bashtag*: **i**) interweaving fibers that formed a basket-weave pattern ([B] *asterisk*), **ii**) fibers oriented radially from the canal ([C] *ampersand*), and **iii**) fibers wrapped circumferentially around the canal ([D] *bashtag*). The radial and circumferential regions form rainbow-colored patterns in their respective directions, making them easily identifiable in the images. As in Figure 3, white lines representing orientation averaged over $20 \times 20 \mu\text{m}^2$ were overlaid to aid discerning the fiber organization.

RESULTS

Figure 3 shows examples of the beautiful architecture of the lamina cribrosa. Collagen fiber microarchitecture can be seen, including beam intersections where the fibers form “knots” with multiple bundles intersecting (Fig. 3B) and fibers that wrap around pores (Fig. 3C). On the lamina cribrosa periphery, we observed two types of lamina cribrosa beam insertions into the sclera (Fig. 3D). Some insertions were narrow, formed by fibers that run perpendicular into the scleral canal. Other insertions were wide, appearing much like old trees, with some fibers running directly into the canal wall and others turning smoothly to integrate with the circumferential fibers of the sclera immediately adjacent to the canal. Note also how robust the PLM technique is able to measure fiber orientations despite substantial pigment (Figs. 3C, 3D), and submicrometer resolution of our imaging and analysis allows direct visualization of the natural waviness of the collagen fibers, or crimp (Fig. 3D). Tracings (Fig. 4) displayed a larger scale collagen organization on the lamina cribrosa, in which some fiber bundles could be traced over distances of up to a millimeter. This is important as it provides a means to study how the lamina cribrosa beams carry and distribute forces. At the pore

scale, the tracings showed collagen fibers wrapped circumferentially around the pores.

Wide-field micrometer-scale maps of collagen fiber orientation over the whole section are shown in Figures 2, 4, 5, and 6, and the quantifications of the fiber orientations in these regions, from eyes fixed at 5 mm Hg IOP, are shown in Figures 7 and 8. The scleral canal and the lamina cribrosa are evident in all images, although the energy masking makes the various structures obvious and interpretation simpler (Fig. 2). Tracings show that different regions of the sclera have specific patterns of collagen fiber orientation, like fibers that extend from the edge of the canal across the whole section (Fig. 4). In Figure 5, 3 distinct regions of the sclera are discernible: **i**) regions of interweaving fibers without a clear orientation; **ii**) circumferential fibers immediately adjacent to the scleral canal; and **iii**) fibers aligned radially to the scleral canal, visible in the most anterior regions of the sclera, which were estimated to be 60 to $180 \mu\text{m}$ thick and extended at least 3 mm from the canal, the edge of the trephined region, clearly seen with long continuous radial fibers in Figure 4A.

These different regions manifested most commonly at different depths in the posterior pole (Fig. 6). To understand the depth-dependence of the fiber architecture, an image stack was formed by manually registering images from all sections of

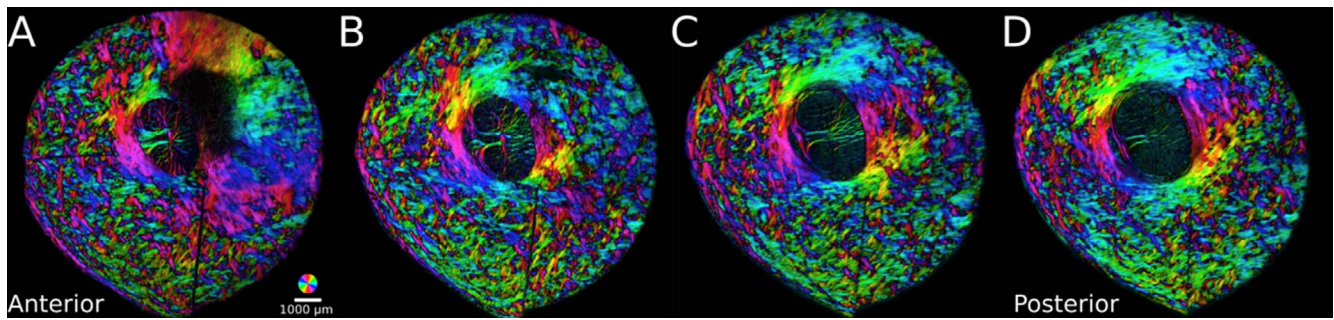


FIGURE 6. Serial optic nerve head sections ordered from anterior to posterior. The radial fibers were found in the most anterior sections (A), whereas the interweaving and circumferential fibers appeared directly posterior and persisted through the sclera (B, C, D). The radial and circumferential fibers are easily distinguishable by the large regions with “rainbow” colors (note the orientation key at the bottom right [A]). The extent of color variation gives an indication of the spatial anisotropy such that large regions of uniform coloring indicate higher anisotropy than regions with much color variations, which suggest more isotropy.

the posterior pole of an eye.²⁶ We manually selected two 467 × 566-μm regions, one proximal to the canal, immediately adjacent to the canal, and another distal, outside the circumferential ring. We then calculated the distribution of fiber orientations in these regions in each section across the tissue depth (Fig. 7). In the anterior-to-posterior direction, radial fibers appear first. In proximal regions, circumferential fibers were directly posterior to the radial fibers (Fig. 7A), and in distal regions, the alignment was much more complex and variable, with interweaving fibers posterior to the radial fibers (Fig. 7B).

Quantitative analysis of the orientation characteristics of the three scleral regions showed distinct differences in collagen

fiber orientation distribution (Fig. 8). Each region was consistently discernable in all eyes and had significant differences in mean orientation and anisotropy ($P < 0.0001$). The radial and circumferential regions were highly anisotropic, differing only on the mean orientation (Fig. 8A), whereas the region of interweaving fibers was much less anisotropic (Fig. 8B) with a corresponding spread mean orientation.

DISCUSSION

Collagen is the main load-bearing component of ocular tissues, and collagen organization has important implications on the ability of the tissues to bear forces, in turn affecting their

Fiber Orientation Through Depth

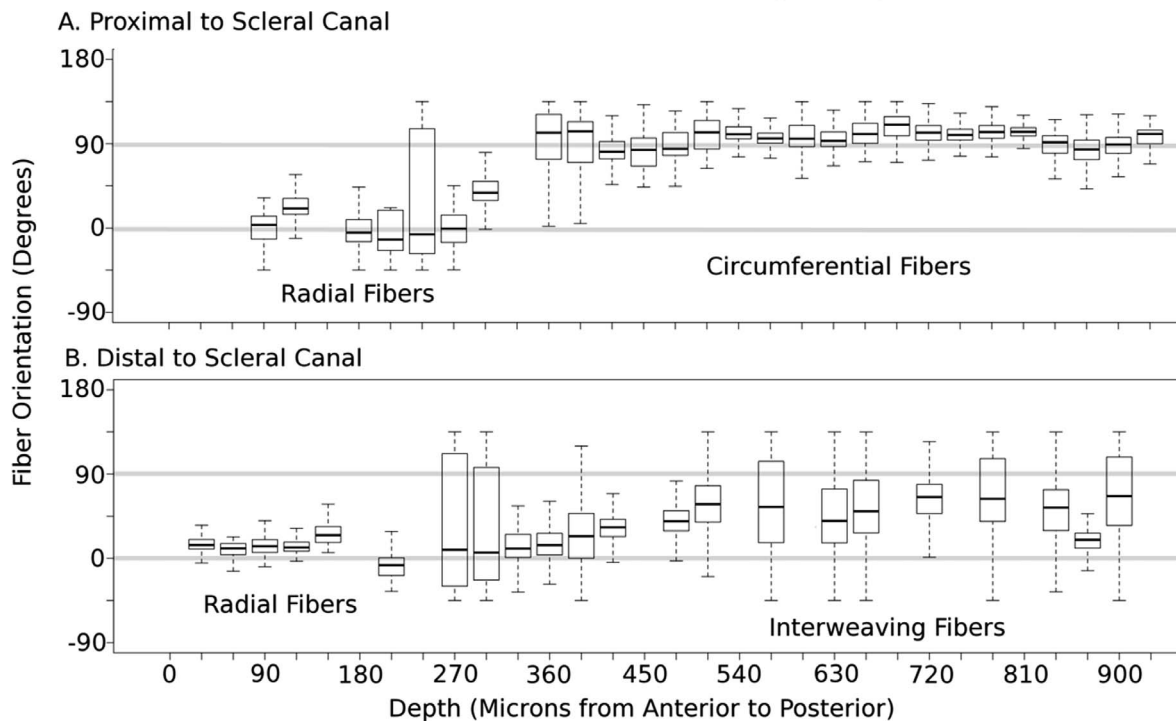


FIGURE 7. Box plots of the polar fiber orientations relative to the center of the canal with depth, from an eye fixed at 5 mm Hg IOP. The circumferential fibers (orientation of 90°) were proximal to the scleral canal (A), whereas the interweaving fibers were distal to the scleral canal (B). No matter the distance from the scleral canal, the most anterior layer was oriented radially (orientation of 0°). The orientation was plotted either from -90° to 90° or from 0° to 180°, depending on which reference frame gave the least variability. Sections with low energy were excluded from analysis.

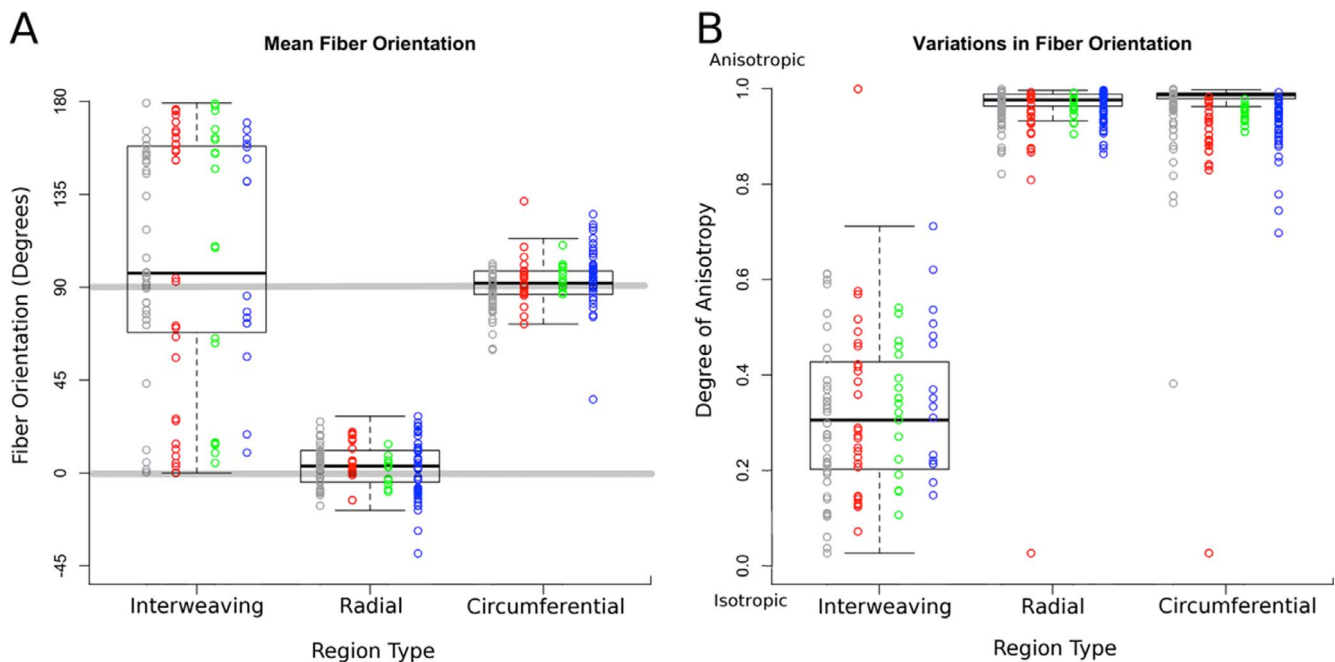


FIGURE 8. Box plots of the polar fiber orientations and degree of anisotropy by region type. Orientation was plotted either from -90° to 90° or from 0° to 180° depending on which reference frame gave the least variability. Data acquired from each sheep were plotted in different columns in different colors. Note that for low anisotropy, the value of the mean orientation has little meaning. Results were consistent between contralateral eyes as well as across eyes from different sheep. All eyes used in this analysis were fixed at 5 mm Hg IOP.

physiology, robustness, and susceptibility to disease. We have presented images of the collagen fiber architecture with micrometer-scale resolution over centimeter-scale regions of the posterior pole including the ONH. With PLM, the various structural components of the ONH and posterior sclera were clearly discernible and could be analyzed with high detail and revealed some characteristics of the collagen architecture that have not been described, and improved clarity of previously described features. Below we discuss some salient examples of our findings, followed by a discussion of the advantages and limitations of the study and of PLM.

The images revealed details of the peripheral lamina cribrosa and of the beam insertions into the scleral canal wall that were either unreported or that had not been characterized in detail. It is through the lamina cribrosa beam insertions into the canal wall that the sclera provides boundary conditions to the lamina cribrosa, transferring forces that can contribute to insult or that provide anchor and support. Hence, the lamina cribrosa beam insertions are critically important for understanding lamina cribrosa biomechanics and biomechanical sensitivity. To the best of our knowledge, there have been no studies that have shown the lamina cribrosa insertions into the scleral canal wall in the way we have shown here. Some studies have addressed the insertion of the lamina cribrosa as a whole.^{26–28} Others studies have described fibers of the lamina cribrosa inserting into concentric circumferential fibers in the sclera,^{29–32} or with fibers running longitudinally within the core of laminar beams.³³ We have shown that some insertions were wide and robust in appearance, with collagen fibers that turned and integrated with those of the sclera resembling old trees. Other insertions were thin and frail-looking, inserting perpendicular to the canal wall. These two beam insertion types may provide different biomechanical support to the adjacent neural tissues and to the capillaries within the beams.³⁴ Insertion types may also be relevant to understand lamina cribrosa disinsertions,³⁵ hemorrhages,³⁶ and progressive remodeling of the lamina cribrosa into the pia mater.^{27,28}

Within the sclera, PLM shows that there are three distinct regions of sclera: circumferential fibers adjacent to the canal, radial fibers on the most anterior sclera, and a less aligned region of interweaving fibers elsewhere. The region of circumferential fibers, often also called the “ring,”²³ has been described by several studies using a variety of methods, including wide-angle X-ray scattering (WAXS),³⁷ SALS,³ second harmonic imaging (SHG),³⁸ scanning electron microscopy,^{32,39,40} immunofluorescence,^{29,30,33} and has been predicted using inverse modeling.¹⁹ Our observation of regions of radial fiber orientation in the sclera confirms a recent report from Pijanka et al.³⁷ The high resolution of PLM allowed us to ascertain that the radial fibers form a layer 60 to 180 μm thick, and the wide field of view shows that this layer can extend at least 3 mm from the scleral canal wall to the edge of the tissue sections. Last, the more isotropic regions of the sclera have previously been identified by SALS³ and predicted by inverse modeling.⁴¹ The combination of high resolution and wide field of view of PLM showed that the fiber bundles form a basket-weave-like pattern with more detail than can be discerned with SALS or inverse modeling. Our findings of variations in collagen architecture with depth are consistent with the descriptions of Thale et al.^{32,39} and Thale and Tillmann⁴⁰ based on images obtained with scanning electron microscopy. They described scleral collagen fibrils arranged in a reticular fashion (low anisotropy) in the external sclera and in a rhombic pattern (high anisotropy) in the internal sclera. The significant differences in orientation characteristics between scleral regions may benefit automated algorithms of segmentation. In terms of the regional biomechanical roles, the circumferential fibers surrounding the scleral canal are generally believed to provide structural strength to the ONH,^{18,41,42} whereas the roles of the radial or interweaving fibers remain unclear and are the subject of current research. Less aligned or isotropic fibers may provide reliable support under a variety of loading conditions, as is observed in tissues such as skin.⁴³ The radial collagen fibers may help reduce mechanical insult to the neural

tissues of the retina that are also organized roughly radially from the ONH.

High spatial and angular resolution afforded by PLM techniques enabled visualization of collagen crimp (Fig. 3D). Collagen crimp has long been established as a key characteristic of fiber-forming collagens that plays a critical role in tissue mechanics at several scales.⁴⁴ Nevertheless, few studies have explored crimp in ocular tissues, and most of what is known about ocular collagen crimp has been estimated from inverse modeling.^{19,41} This is because micrometer-scale resolution is needed for visualizing and measuring the small orientation changes associated with crimp. PLM and our analysis techniques have the appropriate spatial and angular resolution, allowing direct detailed investigation of ocular collagen crimp.²⁰

A valuable advantage of collagen structure analysis based on PLM is that it allows analysis of collagen architecture without the need for labels or stains,^{45,46} dehydration,⁴⁷ or flattening,^{5,23} which can introduce artifacts. Although our technique works well on unfixed samples,²⁰ in this work we used tissues fixed with 10% formalin. We have shown that this fixation has minimal effects on tissue size or shape, an important advantage for morphometry over techniques known to cause substantial shrinkage.⁴⁸

This study is not the first to identify and quantify fiber orientation in these distinct regions of the peripapillary sclera. Some imaging modalities that have been used to quantitatively measure collagen fiber orientation include WAXS, MRI, and SALS. The addition of PLM to the set of analysis tools introduces the possibility of higher resolution, which allows improved precision and accuracy. This study has $\sim 100\times$ the in-plane resolution and $\sim 5\times$ the depth resolution, as well as $\sim 1.4\times$ the angular resolution of a previous study using WAXS, although WAXS has a wider field of view in comparison to the field of view afforded by PLM in this study.³⁷ Compared to MRI,¹⁶ the resolution is $\sim 30\times$ the lateral resolution and $\sim 60\times$ the depth resolution. However, it should be noted that MRI does not require sectioning and can potentially be used to identify collagen microstructural patterns *in-vivo*.^{15,16} Compared to reported SALS resolutions,^{3,49} PLM also has ~ 75 to $200\times$ the in-plane resolution and $\sim 3\times$ the depth resolution (using reported SALS beam diameter and thickness of the ocular tissues analyzed in published reports^{3,4}). Note that our goal was not to do an exhaustive review or comparison of all the techniques available for characterizing collagen fiber architecture in the eye. The techniques can produce useful data, and it may be possible to overcome limitations. For example, improving resolution by changing the illumination beam characteristics.

SHG is a technique that produces micrometer-scale resolution images of collagen in the eye without sectioning or staining.^{38,50,51} Fiber orientation is typically extracted from these images by using gradient-based methods, which calculate the orientation based on the texture in the image. However, high tissue density or pigment can cause artifacts. Quantifying the collagen fiber orientation with PLM is robust to the presence of pigment,²⁰ allowing repeatable imaging of pigmented tissues (Figs. 3C, 3D).

PLM allows quantification of individual lamina cribrosa beams and peripapillary sclera bundles together over a large centimeter-scale field of view, with excellent sensitivity and resolution on both. Many of the imaging modalities listed above are more appropriate to one tissue or the other due to issues with tissue density or feature size. Jones et al.,⁵² for example, used SALS for quantitative analysis of the collagen microstructure of human optic nerve heads over both the lamina cribrosa and the sclera.⁵² The resolution and sensitivity of SALS were sufficient to obtain measurements of the dense circumferential

fibers in the peripapillary sclera. For the lamina cribrosa, however, SALS provided only rough measures of fiber density and a general radial orientation of the beams. Lamina cribrosa insertions could not be discerned or quantified. We have shown that PLM provides excellent quality of data for both lamina cribrosa and sclera, with excellent sensitivity at the critical point of the lamina insertion.

Note that in this study we used three PLM imaging systems. To visualize the fine details of the beams, the lamina cribrosa was imaged with a high-resolution system ($0.73\ \mu\text{m}/\text{pixel}$) using a manual stage. The sclera, however, is much larger and using the manual stage and mosaic stitching would have been very time consuming. Hence, for imaging the sclera we switched to a system with a motorized stage and slightly lower resolution ($0.8\ \mu\text{m}/\text{pixel}$). Quantitative analysis of the radial, circumferential, and interweaving regions required imaging a rather substantial 525 sections. For this task, we selected a system with which we could image a whole section without the need for mosaicking yet with excellent, resolution of $4.1\ \mu\text{m}/\text{pixel}$. We have previously demonstrated that our PLM technique is robust to changes in imaging system and magnification,²⁰ and we confirmed that this was the case for the three setups used in this study (results not shown).

There are several limitations to this study. Sheep eyes have similarities with human eyes, such as a collagenous lamina cribrosa, but they also have differences, such as a thick tree-like structure within the canal called the ventral groove, similar to that of pigs.⁵³ It is possible that some of the structural features we have observed on the lamina cribrosa and sclera are unique to sheep and/or not shared by humans. Although learning about sheep is important to understand as an animal model,⁵⁴ we are working to extend our work to other species. Another limitation is that we used histological tissue sections, which may introduce artifacts, such as warping from sectioning. These effects are small on our cryosectioning process (Tran H, manuscript submitted, 2017) and can, if necessary, be further reduced using fiducials and unwarping techniques.²⁶ Additionally, our study is limited to 2-dimensional (2D) fiber orientations in the section plane. The eye is a complex 3D structure and measurements in 3D may be necessary to determine all the essential characteristics. This is not a limitation specific to our work. The 2D limitation is shared by all the most common techniques for studying the collagen of the eye, such as SALS and WAXS. In fact, the higher lateral and depth resolution of our implementation of PLM compared with the published implementations of SALS and WAXS reduces errors that can arise from the 2D assumption. It is possible that the depth resolution of $30\ \mu\text{m}$ in this study may still not be enough to capture the true orientation. This is because it is possible that multiple fibers with different orientations pass through a single pixel, but our technique would only report the predominant fiber orientation at that pixel. Thinner sections may address some of this concern because higher depth resolution reduces the likelihood of multiple fibers with different orientation passing through the same pixel.

We have leveraged PLM as a powerful technique for visualizing and quantifying collagen fiber architecture in the posterior pole. Our images reveal previously unreported features of the collagen organization of the lamina cribrosa and sclera, and provide improved clarity and more details on features already described. Further work is needed to determine the generality across species of the features identified, as well as the biomechanical roles of the two types of lamina cribrosa beams observed and of the three regions of sclera architecture.

Acknowledgments

The authors thank Jonathan Grimm and Alexandra Gogola for their help developing code.

Supported by US National Institutes of Health Grants R01-EY023966, R01-EY025011, and P30-EY008098 and Canadian Institutes for Health Research operating Grant 1234448.

Disclosure: N.-J. Jan, None; K. Lathrop, None; I.A. Sigal, None

References

- Ethier CR, Johnson M, Ruberti J. Ocular biomechanics and biotransport. *Annu Rev Biomed Eng.* 2004;6:249-273.
- Coudrillier B, Tian J, Alexander S, Myers KM, Quigley HA, Nguyen TD. Biomechanics of the human posterior sclera: age- and glaucoma-related changes measured using inflation testing. *Invest Ophthalmol Vis Sci.* 2012;53:1714-1728.
- Girard MJ, Dahlmann-Noor A, Rayapureddi S, et al. Quantitative mapping of scleral fiber orientation in normal rat eyes. *Invest Ophthalmol Vis Sci.* 2011;52:9684-9693.
- Yan D, McPheeters S, Johnson G, Utzinger U, Geest JPV. Microstructural differences in the human posterior sclera as a function of age and race. *Invest Ophthalmol Vis Sci.* 2011;52:821-829.
- Pijanka JK, Abass A, Sorensen T, Elsheikh A, Boote C. A wide-angle X-ray fibre diffraction method for quantifying collagen orientation across large tissue areas: application to the human eyeball coat. *J Appl Crystallogr.* 2013;46:1481-1489.
- Meek KM, Boote C. The use of X-ray scattering techniques to quantify the orientation and distribution of collagen in the corneal stroma. *Prog Retin Eye Res.* 2009;28:369-392.
- Abahussin M, Hayes S, Knox Cartwright NE, et al. 3D Collagen orientation study of the human cornea using X-ray diffraction and femtosecond laser technology. *Invest Ophthalmol Vis Sci.* 2009;50:5159-5164.
- Coudrillier B, Boote C, Quigley HA, Nguyen TD. Scleral anisotropy and its effects on the mechanical response of the optic nerve head. *Biomech Model Mechanobiol.* 2013;12:941-963.
- Winkler M, Shoa G, Xie Y, et al. Three-dimensional distribution of transverse collagen fibers in the anterior human corneal stroma. *Invest Ophthalmol Vis Sci.* 2013;54:7293-7301.
- Winkler M, Chai D, Kriling S, et al. Nonlinear optical macroscopic assessment of 3-D corneal collagen organization and axial biomechanics. *Invest Ophthalmol Vis Sci.* 2011;52:8818-8827.
- Quantock AJ, Winkler M, Parfitt GJ, et al. From nano to macro: studying the hierarchical structure of the corneal extracellular matrix. *Exp Eye Res.* 2015;133:81-99.
- Quigley HA, Hohman RM, Addicks EM, Massof RW, Green WR. Morphologic changes in the lamina cribrosa correlated with neural loss in open-angle glaucoma. *Am J Ophthalmol.* 1983;95:673-691.
- Quigley HA, Addicks EM. Regional differences in the structure of the lamina cribrosa and their relation to glaucomatous optic nerve damage. *Arch Ophthalmol.* 1981;99:137-143.
- Elkington AR, Inman CB, Steart PV, Weller RO. The structure of the lamina cribrosa of the human eye: an immunocytochemical and electron microscopical study. *Eye.* 1990;4:42-57.
- Ho LC, Sigal IA, Jan N-J, et al. Non-invasive MRI assessments of tissue microstructures and macromolecules in the eye upon biomechanical or biochemical modulation. *Sci Rep.* 2016;6:32080.
- Ho LC, Sigal IA, Jan N-J, et al. Magic angle-enhanced MRI of fibrous microstructures in sclera and cornea with and without intraocular pressure loading. *Invest Ophthalmol Vis Sci.* 2014;55:5662-5672.
- Grytz R, Meschke G, Jonas JB. The collagen fibril architecture in the lamina cribrosa and peripapillary sclera predicted by a computational remodeling approach. *Biomech Model Mechanobiol.* 2011;10:371-382.
- Girard MJ, Downs JC, Bottlang M, Burgoyne CF, Suh J-KF. Peripapillary and posterior scleral mechanics—Part II: experimental and inverse finite element characterization. *J Biomech Eng.* 2009;131:051012.
- Grytz R, Meschke G. Constitutive modeling of crimped collagen fibrils in soft tissues. *J Mech Behav Biomed Mater.* 2009;2:522-533.
- Jan N-J, Grimm JL, Tran H, et al. Polarization microscopy for characterizing fiber orientation of ocular tissues. *Biomed Opt Express.* 2015;6:4705-4718.
- Preibisch S, Saalfeld S, Tomancak P. Globally optimal stitching of tiled 3D microscopic image acquisitions. *Bioinformatics.* 2009;25:1463-1465.
- Heermann DW. Deterministic methods. In: *Computer Simulation Methods in Theoretical Physics.* Berlin Heidelberg: Springer; 1986:13-55.
- Pijanka JK, Coudrillier B, Ziegler K, et al. Quantitative mapping of collagen fiber orientation in non-glaucoma and glaucoma posterior human sclerae. *Invest Ophthalmol Vis Sci.* 2012;53:5258-5270.
- Jammalamadaka SR, Sengupta A. *Topics in Circular Statistics.* World Scientific Publishing Co.; 2001.
- Püspöki Z, Storath M, Sage D, Unser M. Transforms and operators for directional bioimage analysis: a survey. In: De Vos WH, Munck S, Timmermans J-P, eds. *Focus on Bio-Image Informatics.* Switzerland, Basel: Springer; 2016:69-93.
- Sigal IA, Flanagan JG, Tertinegg I, Ethier CR. 3D morphometry of the human optic nerve head. *Exp Eye Res.* 2010;90:70-80.
- Sigal IA, Flanagan JG, Lathrop KL, Tertinegg I, Bilonick R. Human lamina cribrosa insertion and age. *Invest Ophthalmol Vis Sci.* 2012;53:6870-6879.
- Yang H, Williams G, Downs JC, et al. Posterior (outward) migration of the lamina cribrosa and early cupping in monkey experimental glaucoma. *Invest Ophthalmol Vis Sci.* 2011;52:7109-7121.
- Hernandez MR, Luo XX, Igoe F, Neufeld AH. Extracellular matrix of the human lamina cribrosa. *Am J Ophthalmol.* 1987;104:567-576.
- Hernandez MR, Luo XX, Andrzejewska W, Neufeld AH. Age-related changes in the extracellular matrix of the human optic nerve head. *Am J Ophthalmol.* 1989;107:476-484.
- Morrison JC, L'Hernault NL, Jerdan JA, Quigley HA. Ultrastructural location of extracellular matrix components in the optic nerve head. *Arch Ophthalmol.* 1989;107:123-129.
- Thale A, Tillmann B, Rochels R. SEM studies of the collagen architecture of the human lamina cribrosa: normal and pathological findings. *Ophthalmologica.* 1996;210:142-147.
- Morrison JC, Jerdan JA, Dorman ME, Quigley HA. Structural proteins of the neonatal and adult lamina cribrosa. *Arch Ophthalmol.* 1989;107:1220-1224.
- Hayreh SS. Blood supply of the optic nerve head and its role in optic atrophy, glaucoma, and oedema of the optic disc. *Br J Ophthalmol.* 1969;53:721.
- Faridi OS, Park SC, Kabadi R, et al. Effect of focal lamina cribrosa defect on glaucomatous visual field progression. *Ophthalmology.* 2014;121:1524-1530.
- Lee EJ, Kim T-W, Kim M, Girard MJ, Mari JM, Weinreb RN. Recent structural alteration of the peripheral lamina cribrosa near the location of disc hemorrhage in glaucoma. *Invest Ophthalmol Vis Sci.* 2014;55:2805-2815.
- Pijanka JK, Spang MT, Sorensen T, et al. Depth-dependent changes in collagen organization in the human peripapillary sclera. *PLoS One.* 2015;10:e0118648.

38. Winkler M, Jester B, Nien-Shy C, et al. High resolution three-dimensional reconstruction of the collagenous matrix of the human optic nerve head. *Brain Res Bull.* 2010;81:339-348.
39. Thale A, Tillmann B, Rochels R. Scanning electron-microscopic studies of the collagen architecture of the human sclera-normal and pathological findings. *Ophthalmologica.* 1996;210:137-141.
40. Thale A, Tillmann B. The collagen architecture of the sclera-SEM and immunohistochemical studies. *Ann Anat.* 1993;175: 215-220.
41. Grytz R, Meschke G. A computational remodeling approach to predict the physiological architecture of the collagen fibril network in corneo-scleral shells. *Biomech Model Mechano-biol.* 2010;9:225-235.
42. Coudrillier B, Geraldles DM, Vo NT, et al. Phase-contrast micro-computed tomography measurements of the intraocular pressure-induced deformation of the porcine lamina cribrosa. *IEEE Trans Med Imaging.* 2016;35:988-999.
43. Fratzl P. *Collagen: Structure and Mechanics.* Springer Science & Business Media; 2008.
44. Holzapfel GA. Biomechanics of soft tissue. In: Lemaitre J, ed. *Handbook of Materials Behavior Models.* Vol III. Academic Press; 2001;3:1057-1073.
45. Hernandez MR, Luo XX, Igoe F, Neufeld AH. Extracellular matrix of the human lamina cribrosa. *Am J Ophthalmol.* 1987;104:567-576.
46. Hernandez MR, Andrzejewska WM, Neufeld AH. Changes in the extracellular matrix of the human optic nerve head in primary open-angle glaucoma. *Am J Ophthalmol.* 1990;109: 180-188.
47. Yang H, Downs JC, Bellezza A, Thompson H, Burgoyne CF. 3-D histomorphometry of the normal and early glaucomatous monkey optic nerve head: prelaminar neural tissues and cupping. *Invest Ophthalmol Vis Sci.* 2007;48:5068-5084.
48. Downs JC, Yang H, Girkin C, et al. Three-dimensional histomorphometry of the normal and early glaucomatous monkey optic nerve head: neural canal and subarachnoid space architecture. *Invest Ophthalmol Vis Sci.* 2007;48:3195-3208.
49. Zhang L, Albon J, Jones H, et al. Collagen microstructural factors influencing optic nerve head biomechanics. *Invest Ophthalmol Vis Sci.* 2015;56:2031-2042.
50. Kamma-Lorger CS, Boote C, Hayes S, et al. Collagen and mature elastic fibre organisation as a function of depth in the human cornea and limbus. *J Struct Biol.* 2010;169:424-430.
51. Teng S-W, Tan H-Y, Peng J-L, et al. Multiphoton autofluorescence and second-harmonic generation imaging of the ex vivo porcine eye. *Invest Ophthalmol Vis Sci.* 2006;47:1216-1224.
52. Jones HJ, Girard MJ, White N, et al. Quantitative analysis of three-dimensional fibrillar collagen microstructure within the normal, aged and glaucomatous human optic nerve head. *J R Soc Interface.* 2015; 12.
53. Brooks DE, Arellano E, Kubilis PS, Komaromy AM. Histomorphometry of the porcine scleral lamina cribrosa surface. *Vet Ophthalmol.* 1998;1:129-135.
54. Gerometta R, Spiga M-G, Borrás T, Candia OA. Treatment of sheep steroid-induced ocular hypertension with a glucocorticoid-inducible MMP1 gene therapy virus. *Invest Ophthalmol Vis Sci.* 2010;51:3042-3048.